AIAA JOURNAL
Vol. 44, No. 8, August 2006

Stability of Hypersonic Boundary Layer on Porous Wall with Regular Microstructure

A. Fedorov* and V. Kozlov*
Moscow Institute of Physics and Technology, 140180, Zhukovski, Russia
A. Shiplyuk† and A. Maslov‡
Institute of Theoretical and Applied Mechanics, 630090, Novosibirsk, Russia
and
N. Malmuth§
Rockwell Scientific Company, Thousand Oaks, California 91360

Theoretical and experimental studies of hypersonic boundary-layer stabilization using a passive porous coating of regular microstructure are discussed. Propagation of disturbances inside pores is simulated with linear acoustic theory including the gas rarefaction effect. This model provides boundary conditions for stability analysis of boundary-layer disturbances on the porous wall. Experiments were conducted in the Mach 6 wind tunnel on a 7-deg half-angle sharp cone whose longitudinal half-surface is solid and whose other half-surface is covered by a perforated sheet comprising equally spaced cylindrical blind microholes. Hot-wire measurements of "natural" disturbances and artificially excited wave packets are conducted on both solid and porous surfaces. Natural disturbance spectra indicate that the second mode is a dominant instability. The porous coating stabilizes the second mode and weakly affects the first mode. Measurements of artificially excited wave packets show that the porous coating leads to substantial decrease of the wave-packet growth. The experimental data on phase speeds and amplitudes of the second-mode disturbances are compared with theoretical predictions. Satisfactory agreement is obtained for both solid and porous surfaces. This study confirms the concept of hypersonic boundary-layer stabilization by passive porous coatings, which can be used for laminar flow control.

Nomenclature

A	=	disturbance amplitude
A_x, A_y, A_z	=	admittance components
A_θ	=	thermal admittance
C_D	=	$C_D^* \gamma P_e^*$, dynamic compressibility
f	=	frequency
h	=	porous-layer thickness
Kn	=	Knudsen number
M	=	Mach number
Pr	=	Prandtl number
p	=	pressure disturbance
Q	=	mass flux disturbance
Re_{eX}	=	$U_e^* X/\nu_e^*$, local Reynolds number
r_0	=	pore radius
T	=	temperature
U, V	=	mean-flow velocity components
u, v, w	=	velocity disturbance
X, Y, Z	=	hot-wire coordinates
x, y, z	=	Cartesian coordinates
Z_0	=	characteristic impedance
α, β	=	wave-number components
γ	=	specific heat ratio
θ	=	temperature disturbance
Λ	=	propagation constant
μ	=	viscosity
ν	=	kinematic viscosity
ρ	=	density
ρ_D	=	ρ_D^*/ρ_w^*, dynamic density
σ	=	spatial growth rate
ϕ	=	porosity
ω	=	angular frequency

Subscripts

e	=	upper boundary-layer edge
LST	=	linear stability theory
w	=	wall
0	=	initial
∞	=	freestream

I. Introduction

LAMINAR turbulent transition leads to substantial increase of the aerodynamic drag and surface heating of hypersonic vehicles.[1,2] The ability to increase the laminar run is of critical importance in design and optimization of aerospace planes. Aspects of hypersonic boundary-layer transition control are discussed in Ref. 3. Smoothing and shaping of the vehicle surface help to avoid early transition caused by roughness and leading-edge contamination as well as crossflow and Görtler instabilities. However, with these measures, the laminar run might be still short because of the first- and/or second-mode instability.[4,5] The wall cooling, which naturally occurs on hypersonic vehicle surfaces, strongly stabilizes the first mode[6] while it destabilizes the second mode.[7] This indicates that hypersonic laminar-flow-control concepts should address the second-mode instability.

The second mode is associated with instability of trapped acoustic waves of relatively high frequency.[4] Malmuth et al.[8] assumed that a passive ultrasonically absorptive coating (UAC) can stabilize the second mode and, at the same time, can be aerodynamically smooth. This hypothesis was confirmed by the linear stability analyses,[8,9] which showed that the porous UAC causes a massive

Presented as Paper 2003-4147 at the 33rd Fluid Dynamics Conference, Orlando, FL, 23–26 June 2003; received 9 November 2005; revision received 8 February 2006; accepted for publication 9 February 2006.

*Associate Professor, Department of Aeromechanics and Flight Engineering, 16 Gagarin Street. Member AIAA.
†Senior Researcher, 4/1 Insitutskaya Street.
‡Deputy Director, Professor, 4/1 Insitutskaya Street. Member AIAA.
§Senior Scientist, Fluid Dynamics, 1049 Camino Dos Rios. Fellow AIAA.

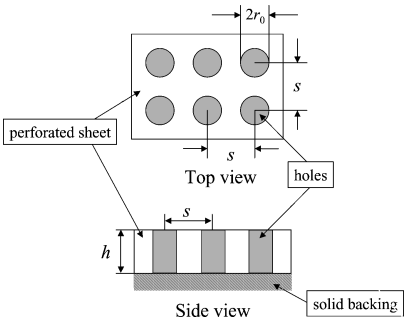

Fig. 1 Sketch of the wall covered by the perforated sheet.

reduction of the second-mode growth rate. The theoretical predictions were qualitatively confirmed by the experiments[10] conducted in the high-enthalpy GALCIT T-5 shock tunnel of California Institute of Technology on a sharp cone at the freestream Mach number $4.59 \le M_\infty \le 6.4$. However, quantitative comparison was not feasible because stability characteristics of the boundary-layer disturbances were not measured. This motivated us to perform a series of stability experiments on cones covered by porous coatings of various microstructures. Further theoretical research was also needed to address randomly porous coatings as well as to account for rarefied gas effects occurring in pores of small size.

The first series of stability experiments was conducted in the T-326 Mach 6 wind tunnel of the Institute of Theoretical and Applied Mechanics (ITAM; Novosibirsk, Russia) on a 7-deg half-angle sharp cone whose longitudinal half-surface was solid and whose other half-surface was covered by a thin porous coating of random structure, namely, a fibrous absorbent material (felt metal).[11,12] Hot-wire measurements of "natural" disturbances and artificially excited wave packets were performed on both solid and porous surfaces. Stability analyses for two- and three-dimensional disturbances showed that the porous coating stabilizes the second mode and marginally destabilizes the first mode. These results are in qualitative agreement with the experimental data for natural disturbances. The theoretical predictions are in good quantitative agreement with stability measurements for artificially excited wave packets associated with the second mode.[11,12]

In this paper, we discuss the second series of stability experiments and calculations, which have been performed for the UAC of regular microstructure (Fig. 1) similar to that tested in the GALCIT T-5 shock tunnel.[10] Some of the discussed hereafter experimental data were used in Ref. 13 for comparison of the UAC efficiencies relevant to coatings of random and regular porosity.

II. Theoretical Modeling

The linear stability analysis is carried out accounting for the mean flow nonparallel effects as described in Ref. 12. The fluid is a perfect gas with Prandtl number $Pr = 0.708$, and the specific heat ratio $\gamma = 1.4$. Viscosity μ is a function of temperature given by Sutherland's formula. The mean flow in the laminar boundary layer is calculated using the conical self-similar solution of boundary-layer equations. The distance X^* from the cone tip is assumed to be much larger than the boundary-layer scale $l^* \equiv \sqrt{(v_e^* X_p^*/U_e^*)}$, where $X_p^* = X^*/3$ according to the Mangler transformation. The ratio $\varepsilon = l^*/X^*$ is treated as a small parameter. The Cartesian coordinates x, y, z are made nondimensional using l^*, and time t and pressure P are referenced to l^*/U_e^* and $\rho_e^* U_e^{*2}$ respectively; other flow characteristics are made nondimensional using their quantities at the upper boundary-layer edge. A three-dimensional monochromatic disturbance is represented by the vector function

$$\boldsymbol{Z} = \left(u, \frac{\partial u}{\partial y}, v, p, \theta, \frac{\partial \theta}{\partial y}, w, \frac{\partial w}{\partial y}\right)^T \tag{1}$$

$$\boldsymbol{Z}(x, y, z, t) = [c(x_1)\boldsymbol{\zeta}(x_1, y, \alpha) + \mathcal{O}(\varepsilon)] \times \exp\left[i\varepsilon^{-1}\int \alpha(x_1, \omega, \beta)\,\mathrm{d}x_1 + i\beta z - i\omega t\right] \tag{2}$$

where u, v, w, p, and θ are velocity components, pressure, and temperature; $x_1 = \varepsilon x$ is slow variable; $(\alpha, \beta) = (\alpha^*, \beta^*)l^*$; $\omega = \omega^* l^*/U_e^*$, $\boldsymbol{\zeta}(x_1, y)$ is the eigenfunction of the local-parallel stability problem

$$\left(\frac{\partial}{\partial y} - \boldsymbol{H}_0\right)\zeta = 0 \tag{3}$$

$$y = 0: \quad \zeta_1 = 0, \quad \zeta_3 = A_y\zeta_4, \quad \zeta_5 = 0, \quad \zeta_7 = 0 \tag{4}$$

$$y \to \infty: \quad \zeta_1, \zeta_3, \zeta_5, \zeta_7 \to 0 \tag{5}$$

The 8×8 matrix $\boldsymbol{H}_0$ is given in the appendix of Ref. 12. Hereinafter the complex eigenvalue $\alpha(x_1, \beta, \omega)$ corresponds to the first or second mode. The amplitude coefficient $c(x_1)$ is obtained from analysis of the next-order problem with respect to ε. The admittance A_y is a complex quantity, which couples the vertical velocity disturbance with the pressure disturbance on the porous surface. On the solid wall $A_y = 0$, and the boundary conditions correspond to no-slip conditions and zero temperature perturbation on the surface of high thermal conductivity.

For the mass-flow disturbance Q, which is measured in experiments, the spatial growth rate σ is calculated as[12]

$$\sigma \equiv \frac{1}{|Q|}\frac{\partial |Q|}{\partial x} = -\mathrm{Im}\alpha + \varepsilon\left(\frac{\partial \ell_n |q|}{\partial x_1} - \mathrm{Im}W\right) + \mathcal{O}(\varepsilon^2) \tag{6}$$

where $q = [\zeta_1 + (\gamma M_e^2\zeta_4 - \zeta_5/T)U]/T$, $W(x_1)$ is relevant to the nonparallel effect. In accordance with experimental measurements, $\sigma(x_1, y)$ is calculated at the level $y = y_m$ of maximum mass-flow disturbance in the boundary layer.

The admittance A_y is expressed in the form[9]

$$A_y = -(\phi/Z_0)\tanh(\Lambda h) \tag{7}$$

where $h = h^*/l^*$ and Z_0 and Λ are the characteristic impedance and propagation constant of an isolated pore, respectively. The latter two are functions of the complex dynamic density ρ_D and the complex dynamic compressibility C_D:

$$Z_0 = \frac{\sqrt{\rho_D/C_D}}{M_e\sqrt{T_w}}, \quad \Lambda = \frac{i\omega M_e}{\sqrt{T_w}}\sqrt{\rho_D C_D} \tag{8}$$

The characteristics ρ_D and C_D are calculated using the model,[14] which is based on solutions describing propagation of disturbances within a long cylindrical tube. This model accounts for gas rarefaction effects, which are important in the case when the molecular mean free path λ^* is not negligible compared with the pore radius r_0^*. As shown in Ref. 14, ρ_D and C_D are

$$\rho_D = \frac{1}{1 - F(B_v, \varsigma)}, \qquad C_D = 1 + (\gamma - 1)F\left(B_E, \varsigma\sqrt{Pr}\right) \tag{9}$$

$$F(B_v, \varsigma) = \frac{G(\varsigma)}{1 - 0.5B_v\varsigma^2 G(\varsigma)}$$

$$F\left(B_E, \varsigma\sqrt{Pr}\right) = \frac{G\left(\varsigma\sqrt{Pr}\right)}{1 - 0.5B_E\left(\varsigma\sqrt{Pr}\right)^2 G\left(\varsigma\sqrt{Pr}\right)} \tag{10}$$

Here $G(\varsigma) = 2J_1(\varsigma)/[\varsigma J_0(\varsigma)]$, $J_{0,1}$ are Bessel functions of the first kind of zero and first order, $\varsigma = \sqrt{(-i\omega^*\rho_w^* r_0^{*2}/\mu_w^*)}$, $B_v = (2\alpha_v^{-1} - 1)Kn$, $B_E = [\gamma(2\alpha_E^{-1} - 1)/(\gamma + 1)Pr]Kn$, α_v is the molecular tangential impulse accommodation coefficient, and α_E is the molecular energy accommodation coefficient. The Knudsen number $Kn = \lambda^*/r_0^*$ is expressed as $Kn = 2\mu_w^*/(\rho_w^*\bar{c}^* r_0^*)$, where $\bar{c}^* = \sqrt{(8R_g T_w^*/\pi)}$ is the mean module of molecular velocity vector and R_g is gas constant per unit mass. Relations (9) and (10) coincide with the known results of the continuum limit $Kn = 0$ (Ref. 15). The latter were used for modeling of the UAC admittance in Ref. 9.

Parametric calculations show that the rarefaction effect leads to increasing of the pore admittance and enhancement of UAC performance. As an example, Fig. 2 shows the second-mode maximum

growth rate, $\sigma_{\max} = \max \sigma(\omega)$, as a function of the longitudinal coordinate for the boundary layer at $M_e = 5.3$, $T_e = 56.4$ K, the local unit Reynolds number $Re_{e1} \equiv U_e^*/\nu_e^* = 2 \times 10^7 \mathrm{m}^{-1}$ and the wall temperature $T_w = T_{\mathrm{ad}}$. Stability calculations for this result assumed the locally parallel theory, that is, the second term in Eq. (6) is neglected. The UAC characteristics are $r_0^* = 25$ μm, $s^* = 100$ μm; the porous-layer thickness $h^* \gg r_0^*$; and the accommodation coefficients $\alpha_v = \alpha_E = 0.9$. At these parameters, which are typical for the wind-tunnel experiment discussed in Sec. III, the Knudsen number is $Kn \approx 0.2$. The second-mode stabilization, predicted at this Knudsen number (dotted line), is stronger than in the case of $Kn = 0$ (dashed line).

III. Experimental Setup and Instrumentation

Experiments were conducted in the open-jet test section of the ITAM T-326 hypersonic blowdown wind tunnel.[16] The diameter of the axisymmetric contoured nozzle was 200 mm. The Mach number in the flow core was $M_\infty = 5.95$. The noise level was ≈1%, which is typical for conventional hypersonic wind tunnels. During the experiments, the total pressure, $P_0 = 10^3$ kPa, and the stagnation temperature, $T_0 = 385$–400 K, in the settling chamber were kept constant with accuracy 0.06 and 0.25%, respectively. The freestream unit Reynolds number was $Re_{1\infty} = (11.5 - 12.3) \times 10^6$ m^{-1}; the wall-temperature ratio, $T_w/T_0 = 0.80$–0.84, approximately corresponded to an adiabatic wall.

The model was a 7-deg half-angle sharp cone of 500 mm length (Fig. 3) consisting of a sharp nose of 65-mm length and 0.1-mm tip radius, a middle portion of 65-mm length with an electric glow-discharge actuator, a base portion of 370-mm length, and a unit providing turning of the cone around its axis. The solid surface roughness was approximately 0.5 μm. The cone was installed at zero angle of attack to an accuracy of 0.05 deg.

The longitudinal half of the base part was covered by a stainless-steel perforated sheet (Fig. 1) that had equally spaced cylindrical holes of depth $h^* = 450$ μm and average spacing $s^* = 100 \pm 4$ μm. The average hole diameter was $d^* = 50 \pm 6$ μm on the face side and $d^* = 64 \pm 6$ μm on the back side (Figs. 4a and 4b), that is, holes were slightly conical with taper angle ≈0.9 deg. The perforated sheet was flush mounted on the cone surface. With the help of a custom-built tension mechanism, the sheet was tightly stretched on to the model to avoid cavities underneath the porous coating. The UAC leading edge was located at a distance $X = 182$ mm ($Re_{eX} \approx 2.8 \times 10^6$) from the cone tip.

The model was equipped with a three-dimensional actuator providing a high-frequency glow discharge in a small chamber. Artificial disturbances generated by the actuator were introduced into the boundary layer through an orifice of 0.4-mm diam located at a distance of 69 mm measured from the cone tip along the cone axis (Fig. 3). The actuator, instrumentation, and measuring system are the same as in the experiment with the porous coating of random microstructure.[11,12] A constant-current hot-wire anemometer was used to measure mass-flow fluctuations. Details of the hot-wire probes and processing techniques are given in Refs. 11, 12, and 17. The amplitude A and phase Φ of disturbances are obtained using the discrete Fourier transformation

$$A(X, Y, \Theta) e^{i\Phi(X,Y,\Theta)} = \frac{2}{N} \sum_{j=1}^{N} \rho U_n(X, Y, \Theta, t_j) e^{-i\omega t_j} \qquad (11)$$

where N is the sample count in the time series, $\rho U_n(X, Y, \Theta, t_j)$ is the time series of mass-flow pulsations, and Θ is the circumferential

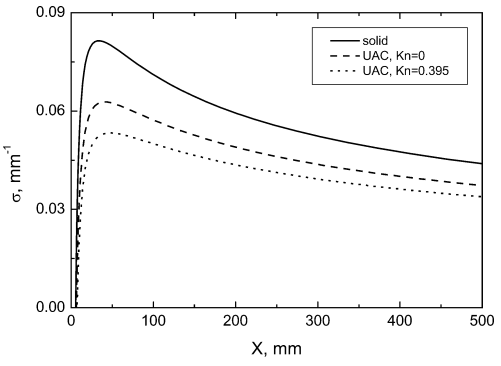

Fig. 2 Rarefaction effect on the UAC performance: $T_w = T_{\mathrm{ad}}$, $Re_1 = 2 \times 10^7$ m^{-1}, $M_e = 5.3$, and $T_e = 56.4$ K.

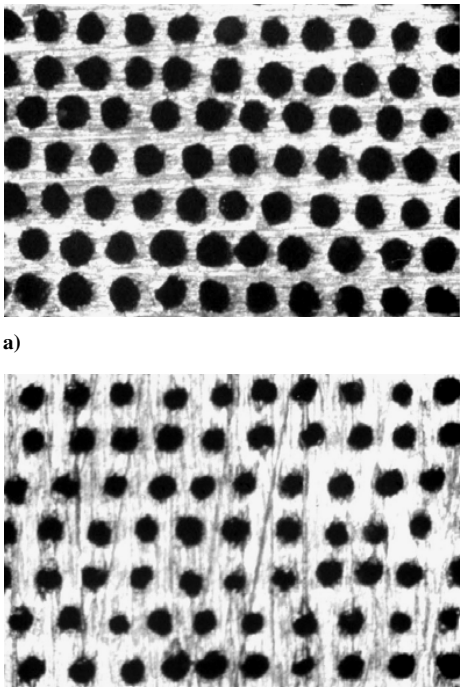

a)

b)

Fig. 4 Micrographs of a) back and b) face sides of the perforated sheet.

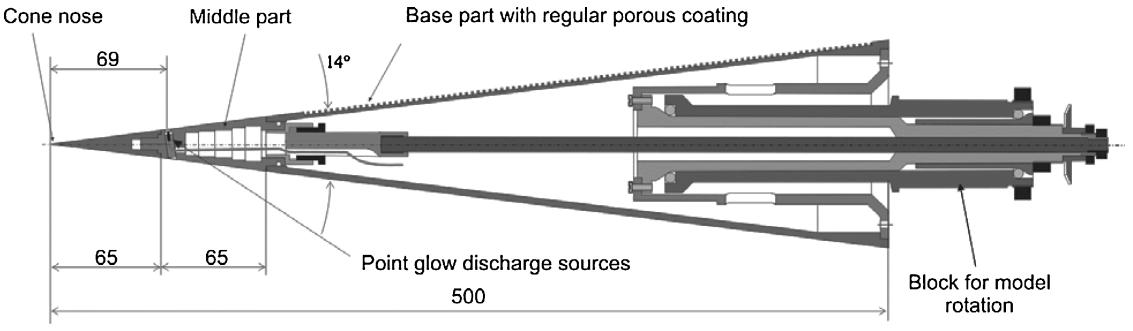

Fig. 3 General view of the sharp cone model.

angle in the cone cross section. The typical number of samples was $N = 4 \times 10^5$.

To compare the experimental and theoretical data, the artificially excited wave packet was decomposed into separate wave components. The transverse wave spectra were calculated as

$$SA(x, \beta)e^{iSF(x,\beta)} = \int_{-\theta_0}^{\theta_0} A(x, \Theta)e^{i\Phi(x,\Theta)}e^{-i\beta\,\Theta}\,\mathrm{d}\Theta \qquad (12)$$

where SA, SF are the amplitude and phase spectra with respect to the transverse wave number β measured in radians/degree. (This unit was chosen because the transversal coordinate was measured in degrees of the circumferential angle in the cone cross section.) A detailed description of the experimental setup, instrumentation, and data processing is given in Ref. 18.

IV. Experimental Results

Hot-wire measurements of mean profiles and rms pulsations of $\rho^* U^* / \rho_e^* U_e^*$ at the stations $X = 138$–287 mm show that the boundary layer is laminar on the solid and porous sides, that is, the porous coating roughness does not cause premature tripping of the boundary-layer flow.

A. Natural Disturbances

Spectra of maximum (vs the vertical coordinate Y) mass-flow disturbances were measured at equally spaced X stations. The first three stations were located upstream of the UAC leading edge. The disturbance spectra $A(f)$ are shown in Figs. 5a and 5b for the solid and porous sides, respectively. Hereinafter the spectrum amplitudes are given in arbitrary units because the calibrated hot-wire data are not available. At the first three stations, the spectra practically coincide on both sides. Downstream of the UAC leading edge, spectrum behaviors are quite different.

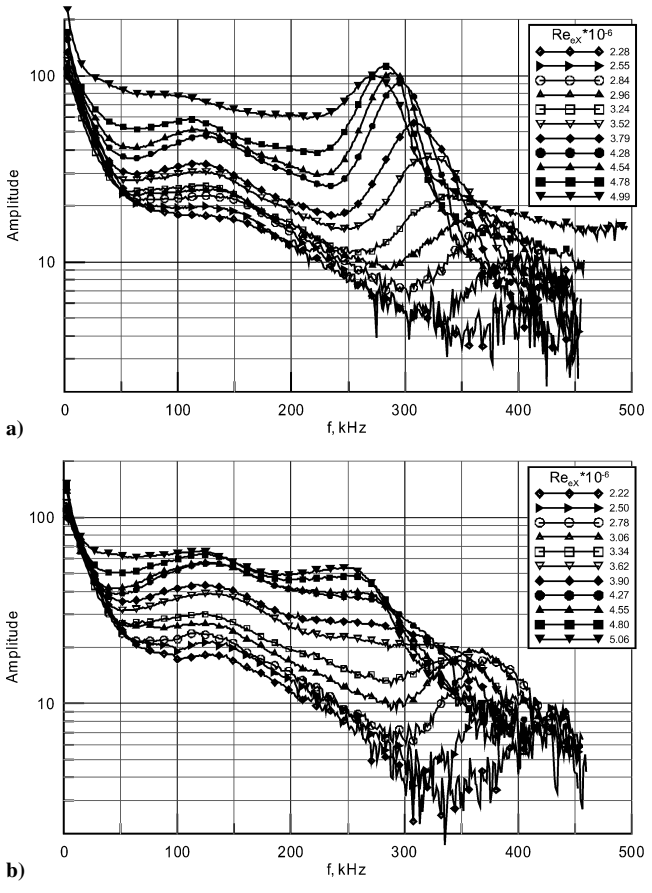

Fig. 5 Natural disturbances spectra in the boundary layer on the a) solid and b) porous sides at various Re_{eX}.

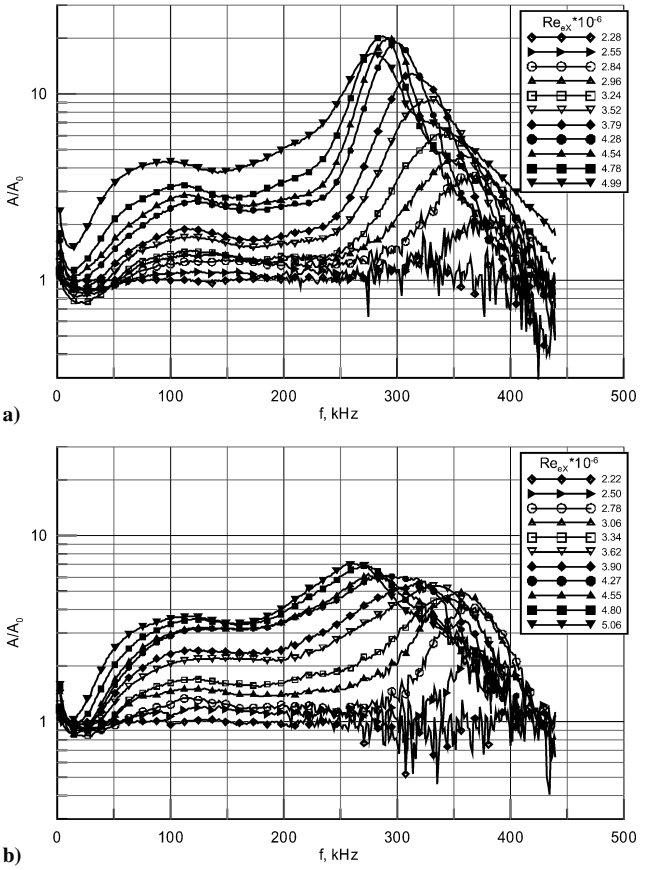

Fig. 6 Normalized natural-disturbance spectra on the a) solid and b) porous sides at various Re_{eX}.

On the solid side, spectra appear very similar to those reported in Ref. 19 for a sharp cone at $M_\infty = 8$. They indicate that the second-mode instability is dominant. At the first upstream station, the second mode was observed at frequencies $\approx$430–450 kHz. Its amplitude quickly increases downstream, whereas its central frequency decreases to 270 kHz at the last station. In the middle of the measurement region ($Re_{eX} \approx 3.42 \times 10^6$), the second mode becomes larger than the first mode associated with the frequency band 50–200 kHz, that is, the first mode grows slower than the second mode. Measurements at the last downstream station (on both solid and porous sides) indicate the beginning of boundary-layer turbulization.

On the porous side, the second mode grows quickly in the first three stations located upstream from UAC. Farther downstream this growth is slowed as a result of the presence of the porous coating. Over the entire measurement region, the second-mode amplitudes are smaller than the first-mode ones.

To evaluate the downstream growth of boundary-layer disturbances, the spectra $A(f)$ are referenced to the initial spectrum $A_0(f)$ measured at the first X station. These normalized spectra A/A_0 are shown in Figs. 6a and 6b for the solid and porous sides, respectively. The first-mode disturbances have nearly equal growth on the both sides, that is, the porous coating weakly affects the first-mode instability. Maximum amplifications are observed in the range 100–130 kHz; they are 3.3 and 3.6 for the solid and porous sides, respectively. The second-mode disturbances grow faster than the first-mode disturbances. Their maximum amplifications are 6.9 and 20.4 on the porous and solid sides, respectively, that is, the UAC effectively stabilizes the second mode.

B. Artificial Wave Packets

Artificial disturbances were generated in the boundary layer at frequency 275 kHz, which is relevant to the maximum amplitude of the second mode measured on the solid side under natural conditions (Fig. 5a). Figure 7 shows transverse distributions of the amplitude at various Re_{eX}. They are nearly symmetric and similar to each other

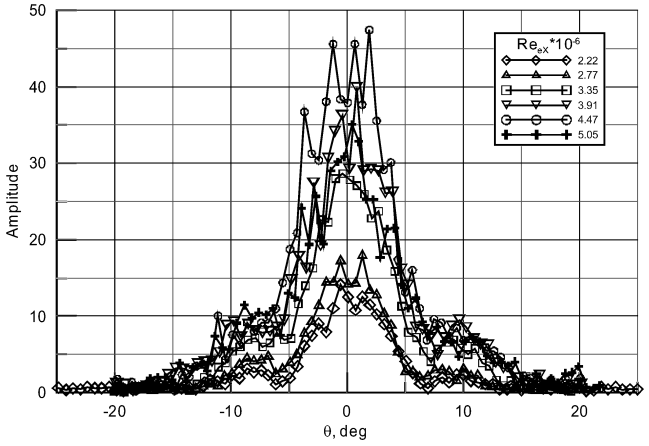

Fig. 7 Transversal distributions of the artificial wave-packet amplitude on the porous side: $\theta \equiv \Theta$.

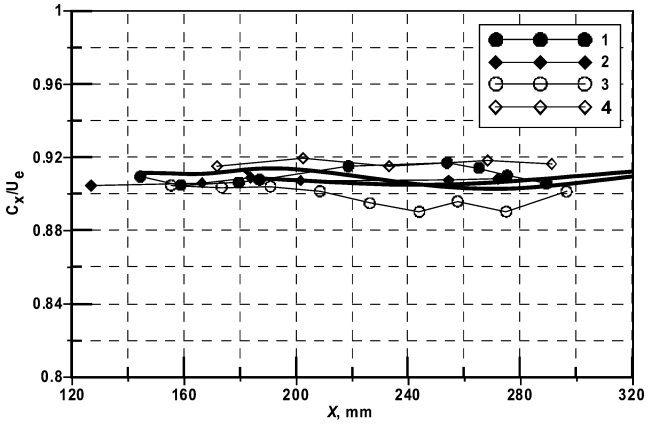

Fig. 8 Phase speeds for artificial disturbances on the porous and solid sides: $f = 275$ kHz; 1 and 2, solid side; 3 and 4, porous side; and thick lines, theory.

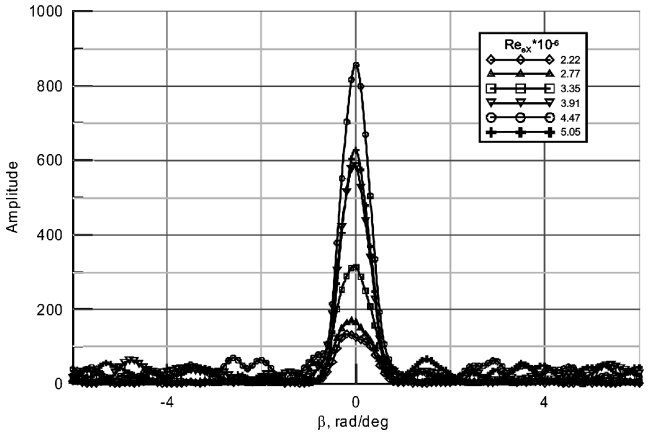

Fig. 9 Amplitude wave spectra with respect to the transversal wave number β on the porous side at various Re_{eX}.

in all cross sections. The amplitude peak at the wave-packet center indicates that the two-dimensional wave component is dominant. The phase distributions are very flat and give nearly constant phase speeds $C_X \equiv C_X^*/U_e^*$ (Fig. 8).

Figure 9 shows the amplitude wave spectra with respect to the transverse wave number β. The wave packets lie within the range $\beta = \pm 0.5$ rad/deg corresponding to the range of the wave-vector inclination ± 20 deg. The amplitude maximums are observed at $\beta = 0$. These features indicate that the dominant component of the artificially excited wave packets is two dimensional.

Amplitudes of natural and artificial disturbances of 275 kHz are shown by symbols in Fig. 10. On the porous side, these amplitudes

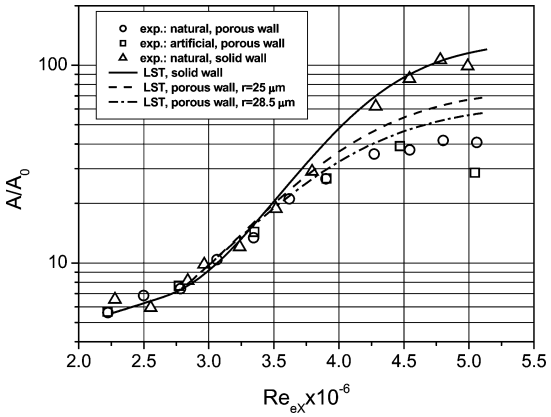

Fig. 10 Downstream development of the second-mode disturbances of frequency 275 kHz.

practically coincide (compare circles and squares), that is, natural disturbances of this frequency are predominantly two-dimensional waves of the second mode. It is clearly seen that the UAC leads to substantial decrease of the amplitude growth. Namely, the maximum amplitude on the porous side (circles and squares) is approximately three times smaller than that on the solid side (triangles).

V. Comparison with Linear Stability Theory

Stability calculations were conducted for two-dimensional disturbances ($\beta = 0$) of the second mode for flow parameters relevant to the experiments. Namely, the local Mach number $M_e = 5.325$, and the wall temperature $T_w = 320$ K corresponds to $T_w^*/T_e^* = 5.471$. The local unit Reynolds number was $Re_{1e} = 15.2 \times 10^6$ m^{-1}; the disturbance frequency $f = 275$ kHz corresponds to the frequency parameter $F \equiv \omega^* \nu_e^*/U_e^{*2} = 1.393 \times 10^{-4}$.

The spatial growth rate was calculated with relation (6) including the nonparallel effect. For the porous wall, stability calculations were conducted using the boundary conditions (4) and (5), in which the admittance is given by Eqs. (7) and (8) with the dynamic density and compressibility (9). The UAC parameters were specified as $r_0^* = 25$ μm, $s^* = 100$ μm, the porosity $\phi = 0.2$, and the porous-layer thickness $h^* = 450$ μm.

Figure 10 compares theoretical amplification curves (solid lines) with the experimental data (symbols). In these calculations, the amplitudes are adjusted to the experimental values at the initial X station. The theory agrees well with the experiment on the solid side (compare the solid line with triangles). The amplification curve calculated for the porous surface (dashed line) lies above the experimental points (circles and squares), that is, the theory underestimates the UAC stabilization effect. Assuming that this discrepancy is caused by the conical shape of actual pores, we calculated the amplification curve for the pore radius averaged over the pore length ($r_0^* = 28.5$ μm). With this correction, the agreement of theory (dashed–dotted line in Fig. 10) with the experiment is satisfactory.

Another factor responsible for the discrepancy between theory and experiment might be nonlinear effects that decrease the second-mode amplification. As mentioned in Sec. IV.A, the nonlinear breakdown of natural disturbances is observed at the last X station. Because amplitudes of artificially excited wave packets are significantly larger than those of natural disturbances, the nonlinear effect can arise earlier. This assumption is consistent with decreasing of the disturbance amplitude at the last station (Fig. 10). Note that the nonlinear aspects of laminar-turbulent transition on a sharp cone with and without the porous coating of regular microstructure are discussed in Ref. 20. The bispectral analysis of the hot-wire signals showed strong subharmonic and harmonic nonlinear interactions over the solid surface. These nonlinear interactions are substantially weakened on the porous surface.

As shown in Fig. 8, the theoretical phase speeds agree well with the experimental data for artificially excited wave packets on both the solid and porous sides of the cone.

VI. Summary

Experimental and theoretical studies of hypersonic boundary-layer stabilization using a passive porous coating of regular microstructure were conducted in order to evaluate the UAC performance for further applications to hypersonic laminar-flow control.

The linear stability problem for disturbances in the boundary layer on a porous wall was formulated using the asymptotic method of multiple scales. This problem differs from the typical stability problem because of new boundary conditions associated with absorption of disturbance energy by the porous coating. The boundary conditions were formulated in terms of the porous-layer acoustic admittances, which depend on the UAC microstructure. Acoustic properties of cylindrical pores were analyzed in the framework of linear acoustic theory including gas rarefaction effects. This analysis is focused on the most practical case when the molecular mean free path is smaller (or much smaller) than the pore radius.

Stability experiments were carried out on a 7-deg half-angle sharp cone with a longitudinal half of its surface solid and the other a porous sheet perforated with equally spaced cylindrical blind microholes. The cone was tested at zero angle of attack in hypersonic freestream of Mach number 5.95. Hot-wire measurements were conducted in the boundary layer on the porous and solid sides of the cone. Spectra of natural and artificially excited wave packets were obtained at various cross sections of the cone.

Measurements of mean profiles and rms pulsations of the mass flow showed that the boundary layer was laminar on the solid and porous sides, that is, the coating roughness did not cause premature transition.

Under natural conditions, the first (low frequency) and second (high frequency) modes were observed in the boundary layer. Analysis of natural-disturbance spectra showed that the second mode was dominant on the solid side. The porous coating stabilizes the second mode and weakly affects the first mode. This observation is consistent with the theoretical predictions.[11,12]

To evaluate the UAC stabilization effect, the wave packets were artificially excited at a frequency relevant to the second-mode instability. It was found that the two-dimensional wave is a dominant component of the wave packets. The amplification of this component nearly coincides with the amplification of natural disturbances of the same frequency. This indicates that natural disturbances in the high-frequency band are predominantly two-dimensional waves of the second mode. It was shown that the UAC leads to substantial decrease of the wave-packet growth. Namely, the maximum amplitude on the porous side is approximately three times lower than that on the solid side.

Stability calculations were conducted for the second mode and compared with the experimental data. The theoretical amplification curve agrees well with the experiment on the solid side. In the case of the porous wall, the theory underestimates the UAC stabilization effect. With a correction accounting for the conical shape of actual pores, the agreement is satisfactory.

In summary, the present theoretical and experimental results confirm the concept of hypersonic boundary-layer stabilization by passive porous coatings. The following issues remain to be addressed in the future:

1) The wall temperatures of actual hypersonic vehicles are substantially lower than the adiabatic wall temperature. Stability calculations[9,11,12] show that UAC performance dramatically increases as the wall temperature ratio decreases. These theoretical predictions need to be verified by stability experiments on a model with a cooled wall.

2) Roughness of the porous coating can lead to premature tripping of the boundary layer. Detailed studies of this detrimental effect will help to formulate criteria for the pore size and spacing.

3) It needs to be shown that the second-mode stabilization leads to an increase of laminar run. At present, we have only indirect experimental evidence in favor of this connection. Namely, the experiments[10] in the GALCIT T-5 shock tunnel showed significant increase of the transition Reynolds number on the porous surface. Further experimental studies are needed to clarify this issue.

4) Refinements of the theoretical model are also needed to address pore end effects, pore-to-pore interaction, and disturbance absorption by coatings of complex microstructures.

Acknowledgments

This effort was supported by the European Office of Aerospace Research and Development under International Science and Technology Center partner Grant 2172. It was also partially supported by the Russian Foundation of Basic Research under Grant 05-01-00349. The authors are grateful to John D. Schmisseur and Steven Walker for support of this research project.

References

[1]Lin, T. C., Grabowsky, W. R., and Yelmgren, K. E., "The Search for Optimum Configurations for Re-Entry Vehicles," *Journal of Spacecraft and Rockets*, Vol. 21, No. 2, 1984, pp. 142–149.

[2]Tartabini, P. V., Wurster, K. E., Korte, J. J., and Lepsch, R. A., "Multidisciplinary Analysis of a Lifting Body Launch Vehicle," *Journal of Spacecraft and Rockets*, Vol. 39, No. 5, 2002, pp. 788–795.

[3]Kimmel, R., "Aspects of Hypersonic Boundary Layer Transition Control," AIAA Paper 2003-0772, Jan. 2003.

[4]Mack, L. M., "Boundary-Layer Stability Theory," *Special Course on Stability and Transition of Laminar Flow*, edited by R. Michel, Rept. 709, AGARD, 1984, pp. 3-1–3-81.

[5]Malik, M. R., Zang, T. A., and Bushnell, D. M., "Boundary Layer Transition in Hypersonic Flows," AIAA Paper 90-5232, Oct. 1990.

[6]Lysenko, V. I., and Maslov, A. A., "The Effect of Cooling on Supersonic Boundary-Layer Stability," *Journal of Fluid Mechanics* , Vol. 147, 1984, pp. 38–52.

[7]Malik, M. R., "Prediction and Control of Transition in Supersonic and Hypersonic Boundary Layers," *AIAA Journal*, Vol. 27, No. 11, 1989, pp. 1487–1493.

[8]Malmuth, N. D., Fedorov, A. V., Shalaev, V., Cole, J., and Khokhlov, A., "Problems in High Speed Flow Prediction Relevant to Control," AIAA Paper 98-2695, June 1998.

[9]Fedorov, A. V., Malmuth, N. D., Rasheed, A., and Hornung, H. G., "Stabilization of Hypersonic Boundary Layers by Porous Coatings," *AIAA Journal,* Vol. 39, No. 4, 2001, pp. 605–610.

[10]Rasheed, A., Hornung, H. G., Fedorov, A. V., and Malmuth, N. D., "Experiments on Passive Hypervelocity Boundary Layer Control Using a Ultrasonically Absorptive Surface," *AIAA Journal*, Vol. 40, No. 3, 2002, pp. 481–489.

[11]Fedorov, A., Shiplyuk, A., Maslov, A., Burov, E., and Malmuth, N., "Stabilization of High Speed Boundary Layer Using a Porous Coating," AIAA Paper 2003-1270, Jan. 2003.

[12]Fedorov, A., Shiplyuk, A., Maslov, A., Burov, E., and Malmuth, N., "Stabilization of a Hypersonic Boundary Layer Using an Ultrasonically Absorptive Coating," *Journal of Fluid Mechanics*, Vol. 479, 2003, pp. 99–124.

[13]Shiplyuk, A. N., Burov, E. V., Maslov, A. A., and Fomin, V. M., "Effect of Porous Coatings on Stability of Hypersonic Boundary Layers," *Journal of Applied Mechanics and Technical Physics*, Vol. 45, No. 2, 2004, pp. 286–291.

[14]Kozlov, V. F., Fedorov, A. V., and Malmuth, N. D., "Acoustic Properties of Rarefied Gases Inside Pores of Simple Geometries," *Journal of the Acoustical Society of America*, Vol. 117, No. 6, 2005, pp. 3402–3412.

[15]Zwikker, C., and Kosten, C. W., *Sound Absorbing Materials*, Elsevier, New York, 1949.

[16]Grigoriev, V. D., Klemenkov, G. P., Omelaev, A. I., and Kharitonov, A. M., "Hypersonic Wind Tunnel T-326," *Aerofizicheskie Issledovania*, edited by A. M. Kharitonov, Inst. of Theoretical and Applied Mechanics, Novosibirsk, Russia, 1972, pp. 16–18 (in Russian).

[17]Maslov, A. A., Shiplyuk, A. N., Sidorenko, A. A., and Arnal, D., "Leading-Edge Receptivity of a Hypersonic Boundary Layer on a Flat Plate," *Journal of Fluid Mechanics*, Vol. 426, 2001, pp. 73–94.

[18]Maslov, A. A., "Experimental and Theoretical Studies of Hypersonic Laminar Flow Control Using Ultrasonically Absorptive Coatings (UAC)," ISTC, Rept. ISTC 2172-2001, Moscow, May 2003 (available from Public Scientific and Technical Information Network, *The DTIC Review*, Vol. 6, No. 4, AD-A423851, URL: http://stinet.dtic.mil/dticrev/vol6-number4.html [cited 8 Feb. 2005]).

[19]Stetson, K. F., and Kimmel, R. G., "On Hypersonic Boundary-Layer Stability," AIAA Paper 92-0737, Jan. 1992.

[20]Chokani, N. D., Bountin, D. A., Shiplyuk, A. N., and Maslov, A. A., "Nonlinear Aspects of Hypersonic Boundary-Layer Stability on a Porous Surface," *AIAA Journal*, Vol. 43, No.1, 2004, pp. 149–155.

A. Tumin
Associate Editor